Towards zero water consumption in solar tower power plants

Carolina Marugán-Cruz[a,*], S. Sánchez-Delgado[a], J. Gómez-Hernández[a], D. Santana[a]

[a]*Energy System Engineering Group (ISE). Department of Thermal and Fluids Engineering. Universidad Carlos III de Madrid, Spain*

Abstract

Important efforts are dedicated to reduce water use in the power generation sector. In this paper the use of a dry Heller cooling system is proposed to diminish the water consumption of a concentrated solar tower power plant. The Heller system is an indirect cooling system where the exhaust steam from the turbine is condensed in a direct contact heat exchanger. Part of the condensate and cooling water are pumped to the feed water heaters while the rest is pumped to the dry cooling tower. In this particular case a natural draft dry cooling tower is employed.

The detailed cycle of the power block and the cooling system have been modeled. The results indicate a reduction of the annual energy production of less than 2% compared to a wet cooling system, and an increase of the energy production by more than 3% compared to a mechanically draft dry cooling system.

A cost model has been presented to determine the equivalent water

*Corresponding author
Email address: cmarugan@ing.uc3m.es (Carolina Marugán-Cruz)

price that makes profitable the use a Heller system (Water price =$1.37\,\$/\mathrm{m}^3$). Furthermore, it has been found that this cooling system is able to reduce almost 1 million cubic meters of water per year, which makes it an attractive choice especially in arid regions.
Keywords: Heller system, Solar Tower, Water consumption, Natural draft tower

---

Nomenclature

Acronyms

CF: Capacity factor

CSP: Concentrated solar power

DC: Direct contact jet condenser

MDDCT: Mechanical draft dry cooling tower

NDDCT: Natural draft dry cooling tower

TDC: Temperature duration curve

Symbols

a: Constant [Pa^{-b}J/kg]

A: Area [m^2]

c_p: Specific heat [J/kgK]

C: Cost [$]

d: Diameter [mm]

D: Tower diameter [m]

ΔT_{lm}: Log mean temperature difference [K]

E: Annual energy production [GWh]

EL: Exhaust losses factor [J/kg]

f: Weighting factor [-]

F_T: Correction factor of the heat exchanger [-]

g: Gravitational aceleration [m/s^2]

H: Height [m]

h_i: Convection coefficient [W/m^{2}K]

h: Enthalpy [J/kg]

k: Pressure loss coefficient [-]

L: Length [m]

$\dot{m}$: Mass flow rate [kg/s]

n, N: Number [-]

p: Pressure [Pa]

P: Pitch [mm]

$\dot{Q}$: Thermal power [W]

R: Gas constant [Pa m^3/kgK]

R_{field}: Field boundary radius [m]

t: Thickness [m]

T: Temperature [K]

TC: Turbine capacity [MW]

U: Global heat transfer coefficient [W/m^{2}K]

V_{an}: Annulus velocity at the last stage [m/s]

V_t: Volume [m^3]

$\dot{W}$: Power [W]

W_{dem}: Water demand

Y: Humidity of the steam at the end line [-]

Greek letters

α: Intersection angle [º]

ρ: Density [kg/m^3]

η: Efficiency [-]

ϵ: Surface roughness [mm]

μ: Dynamic dry viscosity [Pa s]

υ: Specific volume [m^3/kg]

Θ: Semi-angle of the delta columns

Subindex

a: air

c: condenser

e: hydraulic (internal)

f: fin

fr: frontal

HE: heat exchanger

o: outlet of the cooling tower

ref: nominal o reference case

s: shell

t: tube

ts: supports of the tower

w: water

1. Introduction

In Rankine power plants, whether solar thermal, coal or other, the steam coming out of the turbine is condensed to be pumped back to the steam generator. This cooling in the condenser might be done in a wet condenser, a dry cooling tower, or a hybrid system. Due to the superior thermal cooling properties of the water over the air, wet cooling is typically preferred. However, the advantage of dry cooling is that it does not use freshwater: steam is condensed by air cooled condensers or natural draft dry towers that use the ambient air to cool the steam [1].

The use of a dry cooling system has the disadvantage of the reduction in the efficiency and capacity of the power plants. Due to the higher condensing temperature of the steam the efficiency of the Rankine cycle is reduced, and furthermore, since in most of the occasions the dry cooling is performed by mechanical towers the parasitic consumption is higher because of the electricity used by the fans. In mechanical draft dry cooling towers (MDDCT) the air mass flow rate can be controlled by the power of the fans: when the ambient air temperature increases the velocity of the fans can be raised to increase the air mass flow rate. If the condensing is performed by a natural draft dry cooling tower (NDDCT) the cooling air is driven by buoyancy forces and hence, the air mass flow rate is smaller than in mechanical draft tower, and the condensing temperature is higher.

Concentrated solar power, CSP, technology concentrates sun light and converts it into heat, which can be used to produce steam in a Rankine cycle. As a consequence of the better performance of the wet condensers, more than 85% of solar thermal power plants use some sort of wet cool-

ing system [2]. From the 91 commercial CSP for electricity generation, at least 73 use wet or hybrid cooling condensers. However, the best locations for CSP plants are located in sunny regions where there is, often, water scarcity, and most of the new CSP projects use dry cooling condensers [2]. The risk of disruption of local water resources represents the highest environmental risk for CSP projects [3]. As an example, the Hualapai Valley Solar Project in Arizona was not commissioned due to the public opposition to the use of groundwater by the parabolic trough plant [4]. Furthermore, water discharges of CSP plants can negatively affect aquifers [5].

Increases in ambient air and water temperatures lead to reductions in the efficiency and capacity of power plants. It is more that expectable, that due to global warming, both ambient air and water temperatures will increase in future and that this fact can affect the performance of power plants to meet loads. Furthermore, water costs are rising and environmental restrictions are increasing [6], so it is of paramount importance for the further development of CSP to study the most cost effective solution to the cooling system.

So far only a few studies have dealt with the performance of the cooling system in CSP plants. Habl et al. [7] presented an exergoeconomic comparison of a wet and dry mechanical draft cooling tower in a parabolic trough power plant. They concluded that the electricity generation costs of were higher for the air cooling technology. Turchi et al. [8] compared the performance of wet-condenser, mechanically dry air-condensers and hybrid-systems in CSP plants and concluded that the mechanically air-driven condensers reduce the efficiency of the plant and increase the capital costs.

Turchi et al. [8] estimated an increase of the levelized cost of electricity of 2.5% to 9% in parabolic trough power plants using MDDCT. Martín [9] presented the optimization of the operation of a parabolic power plant using MDDCT. The investigator concluded that around 5% of the electricity production was used to provide power to the fans of the A-frame system. Luceño and Martín [10] proposed an optimization procedure for the design of A-frame dry cooling system for CSP plants, and concluded that the optimization could reduce to 4% the energy consumption of the cooling system. The effects of ambient temperature on the performance of a small NDDCT for small CSPs plant was investigated experimentally by X. Li et al. [11]. Furthermore, they modeled the cooling tower to study the effects on Rankine and Brayton cycle, and they showed that the reduction of the efficiency of both cycles was due to different mechanisms. Ehsan et al. [12] proposed the use of a NDDCT for a 25 MW solar plant operated with supercritical CO_2 Brayton cycle. Their study showed that at higher ambient temperature than the design temperature the efficiency of the cooling system was significantly reduced. Other researchers have investigated replacing the condenser by a low temperature multi-effect distillation plant [13]: in these plants the steam at the exit of the turbine is used to feed the desalination plant. In this case the electricity production is diminished due to the reduction of the expansion of the steam at the outlet of the turbine, however, these plants have the advantage that they can simultaneously produce water and electricity.

In this study a natural draft dry cooling tower has been considered. However, this technology is not exempt from some challenges: the height

of these towers forbids their installation near the power block, since their shadow would reduce the solar field efficiency, and therefore they need to be erected at the north of the solar field. However, the steam coming out of the turbine cannot be carried to such a distance. Hence, the use of an indirect dry-cooling system is proposed: the cooling water is used to condensate the turbine exhaust steam, in a direct contact jet condenser. Part of the resultant hot condensate is pumped to an external air heat exchanger, where it rejects the heat to the ambient air and is fed back to the condenser in a closed circuit. This equipment is known as Heller system [14, 15].

The performance of Heller system in traditionally fuel based power plants has been investigated by Ahmadi and Toghraie [16], Jahangiri and Rahmani [17], Jahangiri et al. [18]. Ahmadi and Toghraie [16], Jahangiri and Rahmani [17] investigated the effects of ambient conditions in the energy production of Shahid Montazeri power plant that is cooled by a Heller system. The results of Jahangiri and Rahmani [17] showed that an increase of the ambient temperature above the design temperature affects negatively the net power production. Based on the number of hours that ambient temperature exceeds the design temperature (16.1 °C), the authors determined a reduction of 11% of the total energy production compared to the energy that should have been produced under design conditions during the hot months (from 1st of June to 1st of October).

Jahangiri et al. [18] studied the injection of flue gases of the recovery boiler into the Heller tower.

To the author's knowledge only Colmenar-Santos et al. [19] and Duniam et al. [20] studied the use of a Heller tower in CSP plants. Colmenar-Santos

et al. [19] described qualitatively the advantages of using a Heller cooling system in parabolic trough plants, but they did not model the cycle or the cooling system, so their estimation of the water savings or the cost penalty of the Heller system is not precise. Duniam et al. [20] compared the performance of a direct and indirect NDDCT cooling systems for the heat rejection in supercritical carbon dioxide, sCO_2, Brayton cycle. Duniam et al. [20] concluded that a smaller tower with 40% less heat transfer area are needed in case of an direct NDDCT.

None of the previous studies ([16]-[20]) couple the analysis of a solar tower power plant using a Rankine cycle with a Heller cooling system. The novelty of this work is the evaluation of the net power production and the reduction of water consumption achieved by the Heller NDDCT system in a CSP tower plant. The present study puts forward the economic viability of the implementation of the Heller system based on water costs.

The manuscript is arranged as follows: in section 2, a description of the solar power plant is presented, as well as the detailed thermodynamic cycle and the cooling system model. In section 2.4 the design conditions of the NDDCT are proposed. In section 3 the main results are discussed such as the effects of the operating conditions in the inlet and outlet cooling water temperature or the cycle efficiency. A cost model of the cooling system is presented in section 4, which has been employed to determine the cost of water that ensures the profitability of the Heller cooling system in this type of power plants. Finally in section 5 the most relevant results of the study are summarized and the main conclusions are drawn.

2. Modelling

The CSP plant consists of the following parts: the heliostat field and receiver system, the storage system, the steam generators, the power block and the cooling system. Figure 1 shows the scheme of the power plant. For the condensation of the steam the use of a Heller system is proposed. The numerical model of the power block and the cooling system has been written in MATLAB and the fluid properties are calculated using the Coolprop package [21].

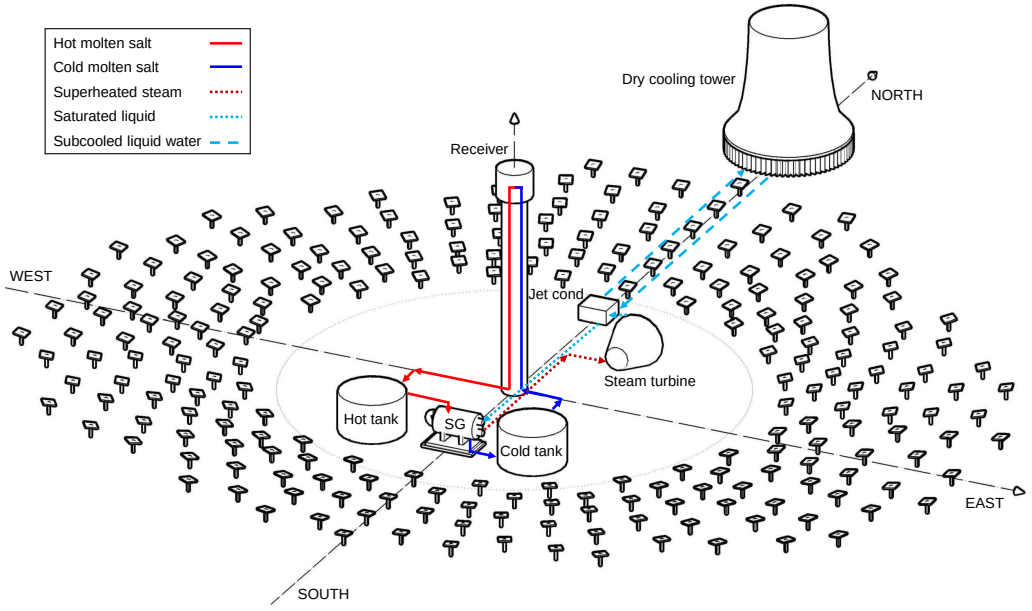

Figure 1: Process flow diagram of the CSP plant with NDDCT.

2.1. Solar system

A molten salt tower power plant, similar to Crescent Dunes, Nevada (USA), has been selected to analyze the performance of the Heller system.

The solar field considered in this study is a radial staggered arrangement with a solar tower at the center (see figure 1). The heliostats or mirrors are located surrounding the tower, and they can be individually oriented to concentrate the solar radiation in the external receiver located at the top of the tower. In the receiver solar radiation is transferred to heat, by conduction and radiation, to the molten salt flowing through it. The salt enters the receiver from the cold storage tank at low temperature (290 °C) and as it moves through the receiver it increases its temperature to 565 °C. The hot salt is then stored in the hot storage tank or sent to the evaporation train. Both cold and hot temperatures are limited by the molten salt freezing point and the decomposition limit, and they delimit the power block efficiency, since the steam high pressure turbine inlet temperature (HPT) is limited to 550 ° C and the temperature at the exit of the last feedwater heater must be above 245 ºC. The two-tank molten salt storage system decouples the electricity production from the solar resource and enable the production of a constant steam mass flow rate. The size of the solar field is designed to produce enough heat to power the turbine and to charge the storage, so in periods of high insolation the incident solar flux in the receiver exceeds the maximum load of the turbine and storage and some heliostats are defocused from the receiver to avoid damages to the receiver. The main design parameters of the solar power plant are described in table 1.

Table 1: Geometrical parameters of the solar system.

Parameter	**Value**
Optical tower height (m)	180
Receiver height, (m)	20
Receiver diameter (m)	17.6
Number of heliostats	10,300
Field boundary radius, R_{field}(m)	1380
North shift of the boundary, Δr_{field} (m)	240
Storage (h)	10

In order to focus the attention on the effects of the cooling system on the performance of these plants, the solar field has not been modeled. It has been assumed that the molten salts are able to produce a constant mass flow rate of steam of 87.46 kg/s at high temperature and pressure, which corresponds to full load conditions of the steam turbine. The details of the power block can be seen in next section.

2.2. Power Block

The power block considered in this work is a reheated and regenerative Rankine cycle, commonly used in CSP plants ([22, 23]). Figure 2 shows the simplified scheme of the power block.

The regeneration of the cycle has been carried out using six closed feedwater heaters (two high pressure feedwater heaters and four low pressure feedwater heaters) and a deareator to preheat the feedwater prior to the steam generator. The variations of the pressure and temperature of both the inlet and outlet of the turbine affects the efficiency of the power block, as well as the amount of thermal power dissipated in the condenser. In this work, the effect of the outlet pressure of the turbine, determined by

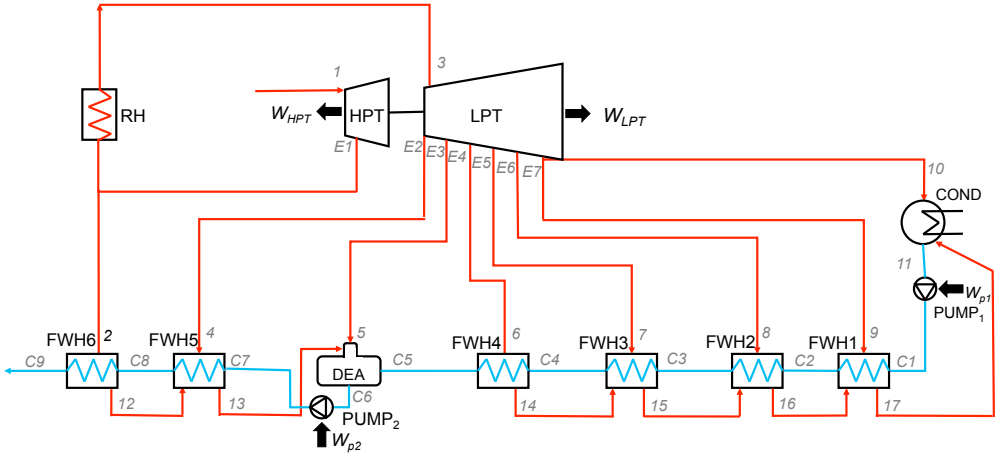

Figure 2: Simplified scheme of the power block. FWH: Feedwater heater. LPT: Low pressure turbine. HPT: High pressure turbine. DEA: Deareator. COND: Condenser. RH: Reheater.

the condenser temperature (saturation conditions), has been analyzed following the previous studies developed by Srinivasan [24] based on the work of Spencer et al. [25]. Table 2 summarizes the operation parameters for the reference case of the power block.

Table 2: Operation parameters of the Rankine cycle at nominal conditions.

Operating Conditions	**Value**
Turbine	
Inlet HPT temperature (°C)	550
Inlet pressure (bar)	126
Reheat LPT inlet temperature (°C)	550
Condensation pressure (bar)	0.1
Extraction point pressures	
Extraction 1, E1 (bar)	36.72
Extraction 2, E2 (bar)	20.47
Extraction 3, E3 (bar)	10.83
Extraction 4, E4 (bar)	5.22
Extraction 5, E5 (bar)	2.21
Extraction 6, E6 (bar)	0.772
Extraction 7, E7 (bar)	0.217
Pressure drops	
Extraction line 1 (%)	2
Extraction line 2, E2 (%)	2
Extraction line 3, E3 (deaerator) (%)	2
Extraction line 4, E4 (%)	5
Extraction line 5, E5 (%)	5
Extraction line 6, E6 (%)	5
Extraction line 7, E7 (%)	5
Extraction end line (%)	5
Boiler (%)	10
Reheating line (%)	5
Condenser (%)	5
Isentropic efficiencies	
High pressure turbine (%)	85
Low pressure turbine (%)	89
Condenser pump (%)	80
Feedwater pump (%)	80
Low/high pressure closed feedwater heaters	
Terminal temperature difference (°C)	1.7/-1
Drain cooling approach (°C)	5.6/5.6

Under nominal conditions, shown in Table 2, the net power produced by the power block is 108 MW_t, and the thermal efficiency of the power

block is $\eta_{T,ref} = 44.1\%$. Under those conditions, at the inlet of the high pressure turbine (HPT) the steam flow rate is 87.46 kg/s and the condensing steam mass flow rate at the end line, $\dot{m}_{el}$ is 61.07 kg/s. In the appendix B the complete energy balance of the power block can be seen in table 2).

End line pressure effect.

The turbine backpressure ranges from 4.9kPa (the shut-off backpressure) to 60 kPa (emergency stop)(Liu et al. [26]). When the condensing pressure is not the nominal condensing pressure (see Table 2), the mass flow rate and pressure of the extraction lines change, varying the net power produced in power block. The method developed by Srinivasan [24] corrects the expansion line end point enthalpy, h_{elep}, as a function of the condensation pressure, as follows:

$$h_{elep} = \Delta h_{elep} + h_{elep,ref} \tag{1}$$

where Δh_{elep} represents the changes in the expansion line end point enthalpy at pressures others that the reference pressure and $h_{elep,ref}$ is the enthalpy end line at the reference pressure. Equation 1 is a nonlinear regression based on the previous work by Spencer et al. [25], where Δh_{elep}:

$$\Delta h_{elep} = a P_c^b + c \tag{2}$$

where $a = 6.266\,10^5$ [J/kg Pa^{-b}], $b = 9.759\,10^{-2}$, $c = -1.441\,10^6$ [J/kg], and

P_c [Pa] is the end-line pressure. The reference end-line reference pressure for Spencer et al. [25] was 5080 Pa, however in this work, the end-line reference pressure is $P_{c,ref} = 10000$ Pa, therefore equation 2 has to be modified to properly calculate the changes in the expansion line for different pressures:

$$\Delta h'_{elep} = \Delta h_{elep} - \Delta h_{ref} \tag{3}$$

where $\Delta h_{ref} = 9.84\,10^4$ J/kg. Therefore, the net power produced in the power block at different end line pressures can be calculated as follows:

$$\dot{W}_{net} = \dot{W}_{ref} - \dot{m}_{el}\Delta h'_{elep} \tag{4}$$

where $\dot{W}_{ref}$ is the net power produced in the reference case, and $\dot{m}_{el}$ is the mass flow rate at the expansion line in the reference case. Equation 5 describes the heat rejected in the condenser

$$\dot{Q}_c = \dot{Q}_{c,ref} + \dot{m}_{el}\Delta h'_{elep} \tag{5}$$

where $\dot{Q}_c$ is the heat rejected in the condensation system at different condensation pressures, and $\dot{Q}_{c,ref}$ is the heat rejected in the condenser in the reference case. Hence, the power block efficiency at different end line pressures is calculated by means of equation 6, where $\dot{Q}_{in}$ is the inlet thermal power of the cycle in the reference case:

$$\eta_p = \frac{\dot{W}_{net}}{\dot{Q}_{in}} \tag{6}$$

Exhaust losses

The steam turbine exhaust loss has to be taken into account in order to quantify the leaving kinetic energy at the exhaust hood of the low pressure turbine (LPT). The exhaust losses (EL) depend on the pressure, mass flow rate, moisture, annulus area and annulus velocity, which raise the turbine exhaust enthalpy, generating a lower enthalpy drop through the turbine. The previous works of Spencer et al. [25], Srinivasan [24], Chacartegui et al. [27], Harvey and Wallace [28] have been used to calculate the called Used Energy End Point, h_{ueep}, as a function of the end line pressure.

$$h_{ueep} = h_{elep} - h_{loss} \tag{7}$$

where

$$h_{loss} = EL \cdot 8.7\,10^{-2}(1 - 0.01Y)(1 - 6.5\,10^{-2}Y) \tag{8}$$

and

$$EL = f(V_{an}) = f\left(\frac{\dot{m}_{el}(1 - 0.01Y)}{\rho A_{an}}\right) \tag{9}$$

where Y is the humidity of the steam at the end line pressure, ρ is the density of the steam at the end line pressure, $\dot{m}_{el}$ is the mass flow at the end line pressure in the reference case and A_{an} is the last stage annulus area. Therefore, equation 6 needs to be corrected to properly calculate the efficiency of the power block at different end line pressure as follows:

$$\eta = \eta_p - \frac{\dot{m}_{el}(h_{elep} - h_{ueep})}{\dot{Q}_{in}} \tag{10}$$

2.3. *The cooling system*

The cooling system proposed in this work is an indirect dry system comprised of a Heller system and a natural draft dry cooling tower. The Heller system uses a direct contact jet (DC) condenser, where the exhaust steam from the turbine is mixed with the water from the cooling tower (see Fig. 3). The typical natural draft dry-cooling hyperbolic tower of concrete shell with vertically delta heat exchangers bundles is shown in Fig. 3.

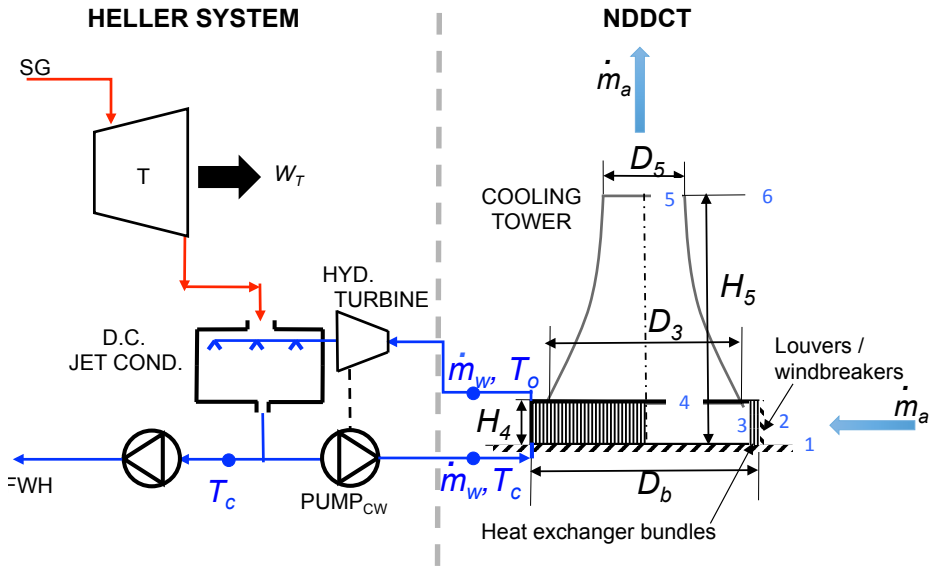

Figure 3: Subsytems of the cooling system: Heller system + NDDCT. **SG** Steam Generator. **T** Turbine. **D.C. JET COND** Direct contact jet condenser. **FWH** Feedwater heater.

In the direct contact jet condenser the water vapour from the turbine condenses on spray droplets. The subcooled liquid water, coming from the tower, is injected through a pressure-swirl nozzle into the condenser chamber with the steam coming from the turbine outlet. At the nozzle exit a thin conical sheet is generated: the liquid has tangential, radial and axial

velocity. At a small distance from the nozzle, the conical sheet breaks into drops of different size and velocity, that reach the saturation temperature.

The condensate partly returns to the cycle and the rest of the liquid is pumped to the NDDCT, where it rejects the heat to the air. Since the NDDCT is typically far from the condenser, to reduce the pumping consumption of the cooling system a hydraulic turbine can be coupled to the pump. The turbine reduces the pressure of the cooling water before entering the condenser tank.

To calculate the air mass flow rate, heat transfer rate, and outlet temperatures of the cooling system a model based on the one dimensional model by Kröger [29] has been developed. It has been validated against the results of presented in Kröger [29] and Conradie [30].

The mechanical power to drive the pump is determined by the pressure differences across the pump due to increasing the pressure above ambient pressure, $\dot{W}_{p,\Delta P}$, the friction losses with distance, $\dot{W}_{p,dis}$, the elevation, $\dot{W}_{p,H}$, and the pressure losses in the heat exchanger, $\dot{W}_{p,HE}$ (see equation 11). The term of the pressure drop in the direct contact heat exchanger has been neglected [31].

$$\dot{W}_{pump} = \dot{W}_{p,\Delta P} + \dot{W}_{p,dis} + \dot{W}_{p,H} + \dot{W}_{p,HE} \tag{11}$$

The details of the calculation of each of the terms in equation 11 are shown in the Appendix A.

The power recovered by the hydraulic turbine can be calculated as follows:

$$\dot{W}_{turb} = \eta_t \dot{m}_w / \rho_w \cdot ((P_{a,1} - P_c) + \rho_w \cdot 9.81 \cdot L_t) \tag{12}$$

The power consumption of the pump-turbine system can be calculated using equation 13:

$$\dot{W}_{pump-turb} = \eta_{e-m} \cdot \left(\dot{W}_{pump} - \dot{W}_{turb}\right) \tag{13}$$

The performance of the NDDCT is affected by the ambient conditions. The performance decreases importantly under high winds or high temperatures. In this study the effect of cross-winds is not investigated. At high ambient temperature the condensing temperature increases reducing the efficiency of the power block. Theoretically, under low temperature the performance should improve, but there is risk of freezing. So under extremely low temperature, to avoid freezing, the power block works with high back pressure, reducing the efficiency of the plant. Researchers have proposed different anti-freezing strategies to operate the NDDCT under very low temperature and cross-winds: Wei et al. proposed controlling degrees of louvers of NDDCT and Yang et al. [33] proposed the use of rolling-type windbreakers, Wang et al. [34] studied switching off sectors and or [34] suggested the using variable-speed pumps to reduce the freezing-risk. In the present work, variable-speed pumps have not been considered because of their high costs.

The mass flow rate of subcooled water that is injected by the nozzles

can be calculated using equation 14:

$$\dot{m}_w = \frac{\dot{Q}_{cond}}{c_p(T_c - T_o) + v\Delta p} \tag{14}$$

where c_p is the specific heat of the liquid, T_c is the saturation temperature and T_o the temperature of the subcooled liquid water coming from the cooling tower. Equation 14 assumes total condensation. This assumption is valid as long as the distance from the nozzle to the well is big enough ([35]).

To determine the subcooled water temperature, T_o, from the the NDDCT, the heat transfer in the tower can be modelled as the convective heat transfer between the water and the tube wall and the convective heat transfer between the tube wall and the air. The conduction heat transfer between the inside and outside of the wall tubes is neglected. The heat transfer in the crossflow heat exchanger can be calculated as:

$$\dot{Q}_{HE} = UA\,F_T\Delta T_{lm} = UA\,F_T\frac{(T_c - T_{a,3}) - (T_o - T_{a,2})}{ln(\frac{T_c - T_{a,3}}{T_o - T_{a,2}}))} \tag{15}$$

where $T_{a,2}$ and $T_{a,3}$ are the air temperatures before and after the heat exchanger respectively (see Fig. 3).

Using the model developed by Kröger [29], the inlet air temperature at the heat exchanger of the NDDCT, $T_{a,2}$, can be approximated to the air temperature at the height of the heat exchanger, $H_4/2$ (eq 16):

$$T_{a,2} = T_a + \frac{dT_a}{dz} \cdot \frac{H_4}{2} \tag{16}$$

where T_a is the dry air temperature at the inlet of the tower, and $\frac{dT_a}{dz}$ is $-9.75\,10^{-3}$ (K/m). The term UA (the product of the overall heat transfer coefficient, U, multiplied by the heat exchanger area) is defined in equation 17 and F_T is the correction factor of the heat exchanger obtained using the explicit equation by Roetzel and Nicole [36].

$$UA = \frac{1}{\frac{1}{h_a\,A_a} + \frac{1}{h_w\,A_w}} \tag{17}$$

where h_a and h_w are the convection coefficient on the air and water side respectively, and A_a and A_w are the external surface area for air and internal surface area for water, respectively. The correlations used to determine the convection coefficients and the internal and external surface areas can be found in the Appendix A, together with an schematic diagram of the heat exchanger (figure A.9).

The heat transfer between the air and the water in the cooling tower can be also calculated as:

$$\dot{Q}_{HE} = \dot{m}_a c_{p,a}\left(T_{a,3} - T_{a,2}\right) = \dot{m}_w c_{p,w}\left(T_0 - T_c\right) \tag{18}$$

Since the system of equations above is non-linear, to solve the heat exchanged in the cooling tower (in equations 15 or 18) initial guess of the subcooled water temperature at the exit of the tower, T_o, is used:

$$T_o^1 = T_c - 15 \tag{19}$$

As a first approximation the mass flow rate of air can be calculated

solving the pressure losses equation in the heat exchanger of the cooling tower (see equation 20).

$$\dot{m}_a^1 = \frac{2 \cdot \rho_{a,23}(\rho_{a,2} - \rho_{a,3}) \cdot g \cdot (H_5 - H_4)}{(K_{HE} \cdot \mu_{a,23}^{b_k} \cdot A_{fr}^{(2+b_k)})^{\frac{1}{2+b_k}}} \tag{20}$$

where $\rho_{a,2}$ and $\rho_{a,3}$ are the dry air density before and after the heat exchanger, $\mu_{a,23}$ and $\rho_{a,23}$ are the air dry dynamic viscosity and density at the air average temperature through the heat exchanger, K_{HE} is the pressure loss coefficient for the air flow through the heat exchanger, A_{fr} is the frontal area of the heat exchanger and b_k is a constant (see Appendix A for details). Once the air mass flow rate is estimated, the air temperature at the exit of the heat exchanger, $T_{a,3}$ can be calculated using equation 21:

$$T_{a,3}^i = T_{a,2} + \frac{\dot{m}_w^i \cdot c_{p,w} \left(T_o^i - T_c\right)}{\dot{m}_a^i \cdot c_{p,a}} \tag{21}$$

However to obtain a more precise value of the air mass flow rate, the rest of the pressure losses need to be taken into account: these losses are due to the presence of other obstacles, supports, contractions and expansions. Additionally, the air flows isentropically between the inlet of the tower and the heat exchanger and between the heat exchanger and the top of the tower. Hence, the total pressure difference between the inlet and outlet of the tower, can be expressed as:

$$p_{a,1} - \left[p_{a,5} + \frac{1}{2\rho_{a,5}} \left(\frac{\dot{m}_a}{A_5} \right)^2 \right] = \sum k_i (\dot{m}_a / A_{fr})^2 / (2\rho_{a,23}) + p_{a,1} \left[1 - \left(1 + \frac{dT_a}{dz} \frac{H_4/2}{T_{a,1}} \right)^{\frac{\gamma}{\gamma-1}} \right] + p_{a,1} \left[1 - \left(1 + \frac{dT_a}{dz} \frac{H_5 - H_4/2}{T_{a,3}} \right)^{\frac{\gamma}{\gamma-1}} \right] \quad (22)$$

where $\gamma = 1.4$ is the heat capacity ratio and $\frac{dT_a}{dz} = -0.00975$ K/m. Equation 22 is known as the *draft equation* [29].

The left side of the draft equation is the total pressure difference between the inlet and outlet of the tower (notice that since the air is stagnant at the inlet, the dynamic pressure does not appear in the expression). On the right side, the first term corresponds to the pressure losses through the different elements of the tower, the second and third term correspond to the pressure difference as the air flows isentropically. The details of the calculation of the loss coefficients, k_i, can be seen in the Appendix A.

Similarly at the top of the tower the temperature of the ambient air conditions can be estimated as:

$$T_{a,6} = T_{a,1} + \frac{dT_a}{dz} H_5 \quad (23)$$

$$p_{a,6} = p_{a,1} \left(1 - \frac{dT_a}{dz} \frac{H_5}{T_{a,1}} \right)^{\frac{\gamma}{\gamma-1}} \quad (24)$$

The density at the outlet of the tower, $\rho_{a,5}$, can be obtained assuming that the pressure at the outlet p_5 is the static pressure at the top of the tower, p_6:

$$\rho_{a,5} = p_{a,6}/(R(T_{a,3} - \frac{dT_a}{dz}(H_5 - H_4/2))) \tag{25}$$

The specifications of the tower size and cooling system can be seen in Tables 3 and 4, respectively. The structure of NDDCT can be of reinforced concrete or aluminum-clad steel, with hyperbolic or cylindrical shape [37]. In general, the hyperboloid geometry offers advantages over other designs, however straight towers, like the NDDCT of the Zayzoon power station in Syria can be also found. As suggested by Duniam et al. [20] the design process of the tower can be simplified if the geometric ratios remain fixed. In Table 3 the chosen ratios can be found. The number of tower supports, n_{sup}, was fixed to 60 independently of the tower size.

Table 3: Fixed geometrical parameters of the cooling tower based on Kröger [29].

Parameter	**Value**
Aspect ratio, H_5/D_3	1.16
Diameter ratio, D_5/D_3	0.57
Inlet height ratio, H_5/H_4	0.13
Number of tower supports, n_{sup}	60

The specifications of the cooling heat exchanger can be seen in Table 4. In this study the heat exchangers are vertical delta radiators at the base of the cooling tower. Each delta radiator is comprised of two columns, with an intersection angle of α. Each column is a plate-fin heat exchanger with the specifications defined in Table 4.

Table 4: Fixed geometrical and thermal parameters of the heat exchanger in the cooling tower based on Kröger [29] and Duniam et al. [20].

Parameter	**Value**
Hydraulic diameter of tube: d_e (mm)	21.6
Wall thickness of the tube: t_t (mm)	2.65
Outside diameter of the tube: d_t (mm)	26.9
Length of the finned tube, L_t (m)	15
Effective length of the finned tube, L_{te} (m)	14.4
Relative surface roughness: ϵ/d_e,	5.24 10^{-4}
Traversal tube pitch, P_t (mm)	58
Longitudinal tube pitch, P_l (mm)	50.2
Fin pitch, P_f (mm)	5.6
Fin root thickness, t_f (mm)	0.3
Number of columns per delta, n_{cd}	2
Intersection angle α (°)	49
Number of tubes per bundle, n_{tb}	284
Number of tubes rows, n_r	4
Number of water passes, n_{wp}	2
Number of plates n_{plate}	2678

Using the parameters of the heat exchanger in Table 4 the total heat exchanger area can be controlled by specifying the number of delta heat exchangers, n_d.

2.4. Design conditions

The design ambient temperature is critical to determine the size of the NDDCT. Selecting a low temperature will reduce the size of the NDDCT (and its initial capital cost) while choosing a higher design-point temperature will increase the efficiency of the power block (and it will increase the

annual income of the power plant). The determination of the design ambient temperature is a trade-off between initial investment costs and the obligations and the penalties included in the contractual commitment.

The Electric Power Research Institute ([38]) proposes to use the summer mean temperature as the design ambient temperature for air-cooled condensers. However, other authors propose different design temperatures: Zou et al. [39] selected as the design point temperature of the NDDCT for a geothermal power plant the ambient hourly average temperature which is equal to or below the temperature for 4500 h in a year, Martín [9] selected as the design point of a MDDCT of a CSP parabolic plant the average temperature of July (the second hottest month), Yang et al. [40], Wei et al. [32] chose much lower design point temperatures. The availability of a CSP plant depends mainly on the sun resource, and for a plant located in the Northern hemisphere the insolation is higher from March to September. For this study the average temperature in that period has been used as design temperature, since the annual average temperature would yield to a too small tower and the EPRI criterion overestimates the size of the tower. In section 3 it can be seen that the NDDCT is able to dissipate the heat during all conditions.

Figure 4 shows the ambient temperature duration curve (TDC) for a typical meteorological year in Tonopah, Nevada (USA). The TDC shows the number of hours that exceed a given temperature: for example, in Tonopah 50 hottest hours exceed 30.85 $^\circ$ C (see Fig. 4). The different design point temperatures described above are shown as well: the average summer temperature is 21.91 $^\circ$ C (magenta circle), the ambient hourly av-

erage temperature which is equal to or below the temperature for 4500 h in a year, that corresponds to 9.48 °C (blue square) or the average temperature from March to September that is 16.4 °C (black diamond).

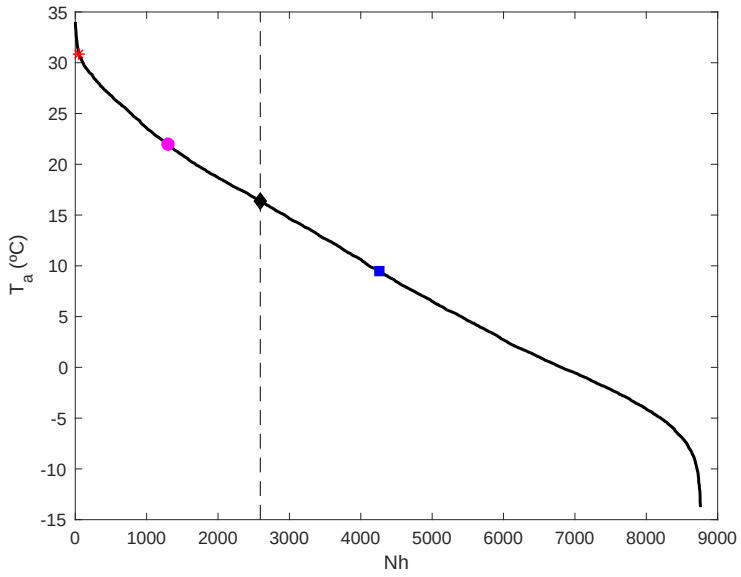

Figure 4: Duration curve based on average data in Tonopah, Nevada. The ambient temperature is plotted against the number of hours above that temperature (black solid line), 50 hottest hours (red star symbol), average summer temperature (magenta circle), and temperature that corresponds to the 4500 hours criterion (blue box). The design temperature, 16.4 °C, is shown as black diamond symbol. The weather data was obtained from the PVGIS database [41].

The cooling mass flow rate is a free parameter, so the velocity of the cooling water inside the heat exchanger was selected to be 1.6 m/s to reduce the fouling and pressure losses, which gives 3800 kg/s of mass flow rate of water through the tower. The tower is designed to be able to reject the condensing heat and return the water to the Heller system at condensing temperature. An initial height of the tower is chosen and the heat rate

dissipated and condensing temperature are calculated, until by an iteration process the height of the tower is obtained.

The tower and heat exchanger dimensions are indicated in Table 5.

3. Results and discussion

The performance of the CSP with Heller-NDDCT cooling system is compared in this section. In Table 5 the specification of the cooling tower obtained from the algorithm proposed in section 2.4 is shown.

Table 5: Geometrical and thermal parameters of the NDDCT.

Parameter	**Value**
Tower total height, H_5 (m)	70
Tower inlet height, H_4 (m)	16
Tower outlet diameter, D_5 (m)	34
Tower inlet diameter, D_3 (m)	60
Length of tower supports, L_{ts} (m)	15
Thickness of the tower shell, t_s (mm)	250
—	—
Number of deltas, n_d	120

3.1. Operating conditions

When the ambient temperature exceeds or is below the design ambient temperature, the performance of the cooling tower will affect the performance of the power block. The interrelation between the heat rejected in the cooling tower and the condensing heat for different condensing temperatures is shown in Fig. 5 for different ambient temperatures. The red line shows the heat rejected at the condenser, $\dot{Q}_c$, for condensing temperatures, T_c. At ambient conditions, T_a = 16.4 °C the heat dissipated by the

NDDCT as function of the water inlet temperature is plotted with a black solid line. The intersection between the two lines defines the designed operating conditions (black diamond). The heat dissipated by the tower when the ambient temperature is below and above the designed ambient temperature is also plotted in Fig. 5. It can be see that when the ambient temperature increases (or decreases) the heat dissipated by the NDDCT changes: the line will move to the right (or left), and the operating point will be the new intersection between the two curves, which will be towards the right (left), this is a higher (lower) condensing temperature and a higher (lower) dissipated heat.

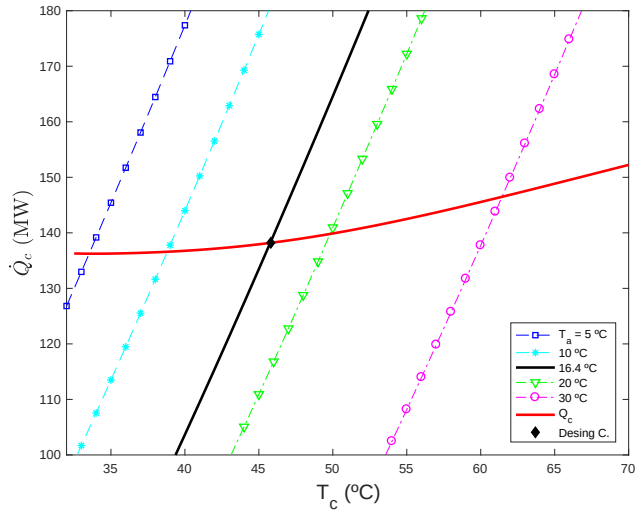

Figure 5: Heat rejection rate in the cooling tower as a function of the condensing temperature for different ambient temperatures: at design conditions (T_a = 16.4 °C): black solid line, under design temperature (dashed lines) and above design temperature (dashed-dot lines). The red line is the condensing heat as a function of the condensing temperature obtained using the method developed by Srinivasan [24].

Figure 6 represents the relation between the inlet (red dashed-dotted

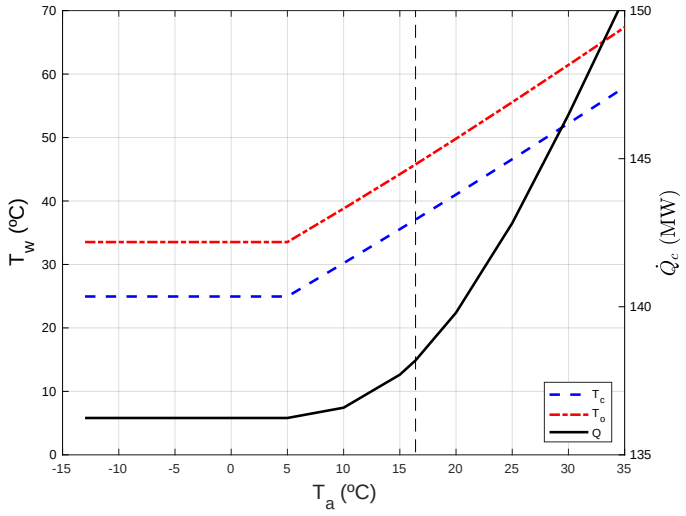

Figure 6: NDDCT performance versus ambient temperature. Left axis: condensing temperature (red dot-dashed line) and cooling outlet water temperature (blue dashed line) and right axis:heat rejected by the NDDCT (black dashed line).

line) and outlet (blue dashed line) cooling water temperature and the ambient temperature (left axis). In this figure the relation of the heat dissipated by the NDDCT with ambient temperature can be seen too. The design conditions are also plotted in the same figure with a vertical dashed line. The NDDCT has been designed to dissipate that heat at design conditions (T_a = 16.4 °C). At design conditions, the condensing temperature is 45.8 °C and the heat dissipated in the condenser is approximately 138 MW. When the ambient temperature increases (or decreases) the temperature of the subcooled water at the outlet of the tower will increase (decrease) too. In the direct contact heat exchanger the mass flow rate of the cooling water and the mass flow rate of the condensing steam mix, and since the first one is much bigger than the latter the condensing temperature increases

(decreases) and therefore the cooling water temperature at the tower inlet is higher (lower) too. Since the condensing temperature is limited to 32.52 °C (p_c = 4.9 kPa), that corresponds to ambient temperature of 5 °C, when the air temperature decays beyond that value sectors of the cooling tower are switched off to prevent damage of the turbine or freezing in the heat exchanger. It is not evident the dependence of the cooling system with ambient temperature, since the heat dissipated in the NDDCT depends on the ambient air temperature and the cooling water inlet temperature, among other variables. As the ambient air temperature increases (decreases), the condensing temperature increases (decreases) too, and hence the condensing heat needed by the power block increases (decreases). Notice that if the ambient air temperature increased and the pumps were provided with a regulator, more water could pumped into the tower to reduce the condensing temperature, in the same way that in a forced air-condenser the fans velocity can be increased to increase the mass flow rate of air.

Figure 7 shows how the ambient temperature affects the mass flow rate of air and the temperature difference between the two inlet fluids (air and water) of the tower. The mass flow rate of the air decreases with ambient temperature while the temperature difference increases. This explains that as the ambient temperature increases the heat rejected by the tower increases, because the variations of temperature are big enough to compensate the reduction of the air mass flow rate.

Figure 8 shows the dependence of the power block efficiency with ambient temperature for a Heller-NDDCT cooling system (blue dashed line) and for a wet cooling tower [42] (black dot-dashed line). In both cooling

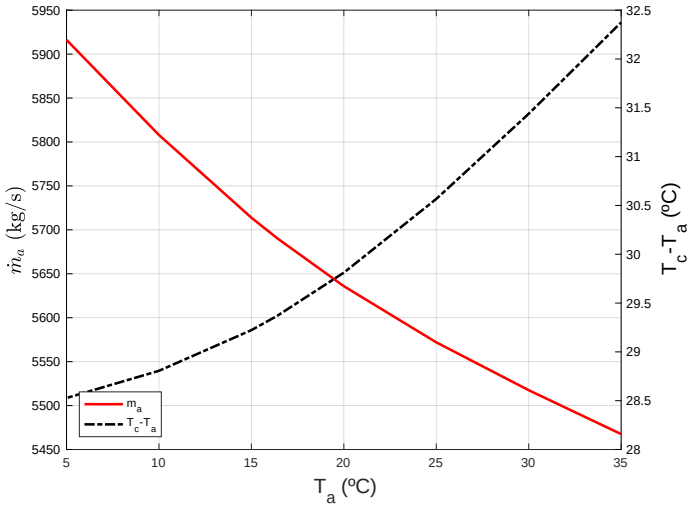

Figure 7: NDDCT performance versus ambient temperature. Left axis: mass flow rate of air (red solid line) and and right axis: inlet fluids temperature difference (black line).

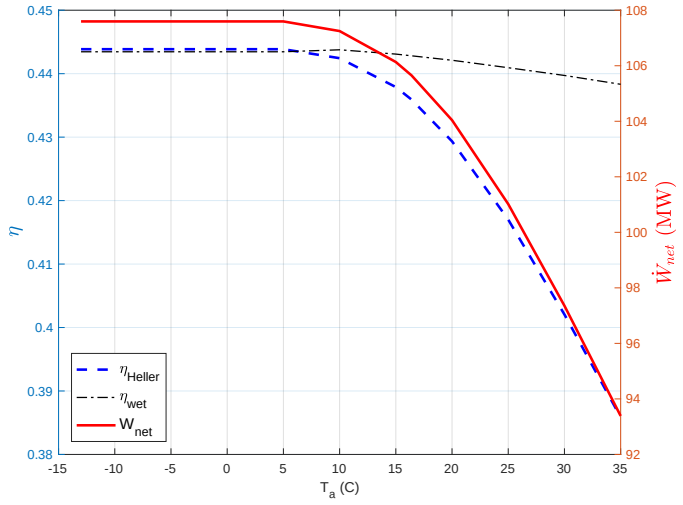

Figure 8: Cycle performance versus ambient temperature. Left axis: efficiency of the cycle using: a Heller-NDDCT cooling system (blue dashed line), or wet cooling tower [42] (black dot-dashed line); and right axis: Net power of the Heller-NDDCT (red solid line)

systems, the efficiency is constant for ambient temperature below 5 °C, since the condensing pressure cannot be further reduced due to the limitations of the shutoff back pressure of the turbine. At temperatures above 5 °C the power-block efficiency decreases with ambient temperature. It can be seen that the reduction of the efficiency with the ambient temperature is more important in the dry cooling system. This is because as the ambient temperature increases, the condensing temperature increases, and the condensing temperature (or pressure) affects the efficiency of the power block: the higher the condensing the lower the efficiency.

In the right axis of Fig. 8 the effect of the ambient temperature on the net power produced by the CSP tower plant with the Heller-NDDCT cooling system can be seen. At low temperatures (below 5 °C) the net power is constant and maximum, while for higher ambient temperatures the net power produced by the plant decreases. In the Appendix B the hourly performance of the Heller-NDDCT and the net power produced a the power block for three different days can be seen.

The annual energy production of the plant can be estimated approximately using equation 26, where Nh_i is the number of hours at a certain temperature obtained from the duration curve based on average data in Tonopah (see Fig. 4), and CF is the planned capacity factor for Tonopah (CF = 51.89%, [2]). The capacity factor is the plant electricity energy output to the maximum possible electrical energy output over a period of time. In the case of CSP plants the factor that affects mostly the CF is the availability of the energy resource (the sun radiation).

$$E_{an,Heller} = \sum \mathrm{Nh}_i(\eta_i \cdot \dot{Q}_{in} - \dot{W}_{pump-turb}) \cdot CF \tag{26}$$

Since the Heller system is an indirect cooling system where cooling water needs to be pumped to the NDDCT to condense the steam, and hence the energy consumption in the pumping system,$\dot{W}_{pump-turb}$, needs to be taken into account. The annual energy production of the CSP tower plant with the Heller-NDDCT cooling system is 484.733 GWh. Compared to the 500.000 GWh/year originally planned [2] it means a reduction of 1.54% of the total energy and less than 2% compared to a wet-cooling system. In the case of solar plants with air-cooled condensers the annual energy production is reduced due to the power consumption of the fans in these equipments. Bracken et al. [4] estimate a reduction of the efficiency of these plants of 5 % in hot climates ($\eta_{MDDCT} = 95\%$). Hence the annual energy production for the CSP plant with mechanically driven air cooled condensers can be calculated as:

$$E_{an,dry} = \sum \mathrm{Nh}_i(\eta_i \cdot \dot{Q}_{in})\eta_{MDDCT} \cdot CF \tag{27}$$

Hence, the annual energy production of the CSP tower plant with a MDDCT is 469.355 GWh, which is a reduction of approximately 3.2% in the annual energy production compared to a Heller system. To quantify precisely the energy produced, the water saved and the profitability of different cooling systems, an annual simulation of the solar field, storage system and power-block will be performed as future work.

4. Cost model

In order to perform an economic analysis of this cooling system a cost model has been developed based on the models of Conradie [30] and Zou et al. [39]. The costs of the NDDCT, the Heller system and the circulating system are taken into account.

The calculation of the NDDCT costs are based on the tower and the heat exchanger costs. The cost of the tower is comprised of the cost of the concrete shell, C_{shell}, the tower foundation, C_{found}, the towers supports, $C_{support}$, and the labour costs, $C_{tow,labour}$:

$$C_{tow} = (C_{shell} + C_{found} + C_{support} + C_{tow,labour}) \cdot f_{st,maint} \tag{28}$$

where $f_{st,maint}$ is the structural maintenance weighting factor.

According to Kloppers and Kröger [43] the capital cost of the tower shell can be approximated by:

$$C_{shell} = C_{conc} \cdot V_t \tag{29}$$

where C_{conc} is the cost of the concrete structure including the cost of construction, $C_{conc} = 200$ \$/m^3 ([44]), and V_t is the volume of the concrete tower shell as the difference between 2 conical frustum.

The cost of foundation includes the land, excavation and foundation costs, as given by equation 30:

$$C_{found} = f_{found} \cdot D_3 \tag{30}$$

where f_{found} is the foundation costs per unit of length.

Additionally, the cost of the tower supports can be determined using the equation 31, proposed by Zou et al. [39]:

$$C_{support} = C_{found} \cdot f_{support} \tag{31}$$

where $f_{support}$ is the ratio of the support cost to the foundation cost.

Finally the labour costs of the tower are proportional to the material cost of the shell, foundation and supports:

$$C_{tow,labour} = (C_{shell} + C_{found} + C_{support}) \cdot f_{tow,labour} \tag{32}$$

Similarly the costs of the finned heat exchanger bundles, C_{HE} can be calculated as the costs of the finned tubes, C_{f-t}, header, C_{header} and labour costs, $C_{labour,HE}$ [39].

$$C_{HE} = (C_{f-t} + C_{header} + C_{labour,HE}) \cdot f_{he} \tag{33}$$

The cost of the finned tubes bundles of the heat exchangers can be calculated using equation 34:

$$C_{f-t} = (C_f \cdot n_{plate} + C_t \cdot n_{tb}) \cdot n_d \cdot n_{cd} \cdot L_t + C_{header} \tag{34}$$

where C_f is the cost of the fins:

$$C_f = (W_f \cdot T_f - n_{tb} \cdot \pi \cdot d_t^2) t_f \cdot \rho_{al} \cdot C_{u,al} + C_{af} \tag{35}$$

C_t is the tube cost per unit of length:

$$C_t = \pi \cdot (d_t^2 - d_e^2)/4 \cdot \rho_{steel} \cdot Cu_{steel} + C_{at} \tag{36}$$

and finally the header costs can be determined as a fraction of the costs of the finned tubes:

$$C_{header} = C_{f-t} \cdot f_{header} \tag{37}$$

The labour costs of the heat exchanger are taken into account:

$$C_{HE,labour} = (C_{f-t} + C_{header}) \cdot f_{HE,labour} \tag{38}$$

As explained above, the Heller system is composed of a direct-contact condenser and the pump-turbine system (see Fig. 3). The pump-turbine system typically consists of a turbine, two pumps ($n_{pump} = 2$) operating at 50% of duty and an electric motor. The cost of all these elements needs to be taken into account:

$$C_{Heller} = (C_{DC} + n_{pump} \cdot C_{pump} + C_{turb} + C_{e-m}) \tag{39}$$

The cost of the pumping system depends on the power of the pump:

$$C_{Pump} = C_{pump,fx} + \dot{W}_{pump} \cdot C_{u,pump} \tag{40}$$

where $C_{pump,fx}$ and $C_{u,pump}$ are the fixed and unit costs of the pumps.

Finally, the investment cost of the turbine, C_{turb}, has been estimated to be as that of the pumps and the motor cost is related to the corresponding pump cost by the factor f_m.

$$C_{e-m} = C_{Pump} \cdot f_m \tag{41}$$

555 *4.1. Costs analysis and water savings*

556 In Table 6 the costs of each subsystem are shown. They have been cal-
557 culated with cost data used in Table A.7. It can be noticed that the biggest
558 costs are the NDDCT and the heat exchanger and that the total investment
559 cost, C_{Tot}, of the cooling system proposed is 12.70 M$.

Table 6: Detailed costs of the cooling system.

Parameter	**Value**
Cost of tower shell	0.51 M$
Cost of tower foundation	1.34 M$
Cost of tower supports	0.11 M$
Cost of Tower labour cost	0.98 M$
Total investment costs of NDDCT	3.53 M$
Total Heat exchanger cost	6.70 M$
Direct contact condenser	0.42 M$
Cost of pumps	0.64 M$
Cost of electric motor	0.35 M$
Cost of turbine	0.32 M$
—	—
Total costs of the Heller + NDDCT system , C_{Tot}	12.70 M$

560 The Heller cooling system is a relatively expensive option. Compared
561 to mechanical dry air-cooled condensers the investment costs are similar
562 [42, 45, 46], but compared to wet-condensers the Heller systems are ex-
563 pensive. In the literature [9] it is reported that dry cooling systems can be
564 1.85 times more expensive than wet-condensers. However, the advantage

of the Heller + NDDCT system is that it uses a closed water circuit for condensing the steam out of the turbine and, therefore, water consumption is minimum, while CSP plants using wet condensers involve great volumes of water being evaporated. This fact can turn the Heller system into an appealing option when the fresh water is not available or it is too expensive.

The reduction in the water consumption in a concentrated solar tower plant condensed by a Heller cooling system depends on the on the turbine capacity, TC, and the capacity factor of the power plant, CF. According to Damerau et al. [47] in hot regions, such as North Africa, the water demand, W_{dem}, of central tower solar systems operating with wet cooling can be up to 2340 m^3/GWh. Hence, the annual water saved can be determined using equation 42:

$$\text{Water Saved} = CF \cdot TC \cdot 24 \cdot 365 \cdot W_{dem} \cdot f_{cond} \tag{42}$$

where f_{cond} is the ratio of the water used in the condenser to the total water consumption. In solar tower power plants around 90 % of the water used in wet cooling CSP plants is used in the condenser [8, 48].

The planned capacity factor of Crescent Dunes was 51.89% (500000 MWh/year) however in 2018 the energy produced by the plant was 195.818 GWh ([49]) that corresponds to a plant capacity of 20.32 %. It is foreseeable that the plant will achieve its planned capacity in the next years, which means that the water consumption for the 108 MW CSP plant with wet cooling plant could be $9.85 \cdot 10^5$ m^3 of freshwater a year.

The breakeven cost of water is the point where the total lifetime cost of

a dry cooling system equals the total cost of a wet cooling system (Maulbetsch and DiFilippo [50]). Hence, a simple conservative economic analysis is to estimate the price of the cubic meter of freshwater for the Heller system to be profitable. This breakeven water cost can be obtained using equation 43:

$$\text{Water Price} = \frac{(C_{Tot} - C_{Tot}/1.85) + (E_{an,wet} - E_{an,Heller}) \cdot N_{years} \cdot PPA}{\text{Saved Water} \cdot N_{years}} \quad (43)$$

where N_{years} is the lifetime of the heat exchanger, that is expected to be 25 years and $PPA = 0.135\,(\$/\mathrm{kWh_e})$ is the power purchase agreement for Crescent Dunes [51]. The first term in equation 43, $(C_{Tot} - C_{Tot}/1.85)$, is the difference of the investment costs and the second term considers the different revenue of the Heller condensed CSP plant, due to the smaller energy production compared to a wet condensed plant. The Heller system can be considered an alternative to wet cooling as long as the price of fresh water is higher than $1.37\,\$/\mathrm{m^3}$.

5. Conclusions

The performance of Heller cooling system with a natural dry draft cooling tower for a solar power tower has been investigated. The NDDCT and heat exchanger sizes were selected to meet the design condenser heat duty at an ambient temperature of 16.4 °C, which corresponds to the average temperature from March to September.

A model for the off-design performance of the cooling system has been developed to investigate the influence of the ambient temperature on the condensing heat, the efficiency and net the power produced. A cost model has been presented to evaluate the costs of the cooling system.

Based on the present analysis, the following conclusions can be drawn:

- The annual energy production of a CSP tower plant using a Heller-NDDCT cooling system is only 2% smaller compared to a wet cooling system, because of the lower condensing temperature achieved by the wet cooling systems. On the other hand, the Heller-NDDCT cooling system is capable of increasing by more than 3% the annual energy production compared to a mechanical draft dry cooling system.

- The advantage of indirect air cooling system is the reduced water consumption compared to the wet cooling system that is commonly used in CSP plants. Furthermore, the Heller cooling system can be considered as an alternative to the traditional wet cooling tower, not only in very dry areas, but also in other regions of the world as long as the price of fresh water is considered. An equivalent water cost of $1.37\,\$/\mathrm{m}^3$ makes the Heller system the best alternative.

Acknowledgements

The authors gratefully acknowledge the financial support given by the Spanish Ministerio de Ciencia, Innovación y Universidades (RTI2018-096664-B-C21 (MICINN/FEDER, UE)).

Appendix A.

Figure A.9 shows the geometric details of the 4-row staggered flat finned tube bundles.

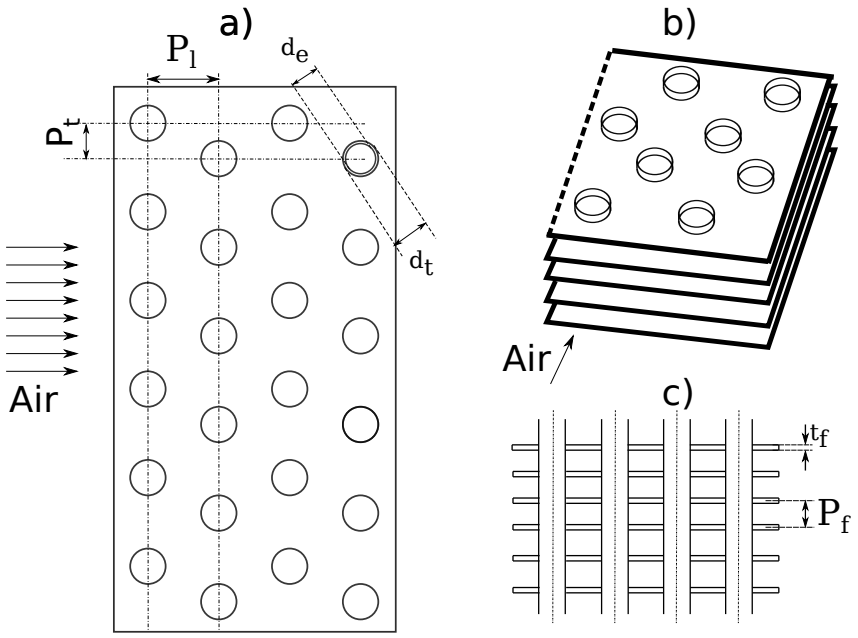

Figure A.9: Simplified scheme of the heat exchanger. a) Geometric details of the finned tube bundles. b) Schematic diagram of the heat exchanger (for saving space only two tubes per row are shown) c) Cross-section in the fin perpendicular plane.

The correlation of Kong et al. [52] for flat finned tube bundles was used to calculate the heat transfer coefficient for the air side.

$$Nu_a = \frac{h_a d_t}{k_a} = 2.6653 \cdot Re_{d_t}^{0.3175} \cdot (P_t/d_t)^{-0.8732} \cdot (P_l/d_t)^{-0.5618} \tag{A.1}$$

where Nu_a and Re_{d_t} are the Nusselt and Reynolds numbers for the air

flow. Notice that in equation A.1 the Nusselt number is defined with the average heat transfer coefficient taking into account the fins.

$$h_a = \left[1 - \frac{A_f}{A_a}(1 - \eta_f)\right] h_e \tag{A.2}$$

where η_f is the efficiency of a single fin and A_f is the entire fin surface area.

For the water side:

$$Nu_w = f_{dw}/8 \cdot (Re_w - 1000) \cdot Pr_w \cdot (1 + (d_e/L_{te})^{0.67}) / (1 + 12.7 \cdot \sqrt{(f_{dw}/8)} \cdot (Pr_w^{0.67} - 1)) \tag{A.3}$$

where Nu_w, Re_w and Pr_w are the Nusselt, Reynolds and Prandtl numbers for the water flow, and f_{dw} is the friction factor:

$$f_{dw} = \frac{0.3086}{log_{10}(6.9/(Re_w) + (5.24\,10^{-4}/3.7)^{1.11})^2} \tag{A.4}$$

The contact area of the heat exchanger:

$$A_a = [2(W_f \cdot T_f - \pi/4 \cdot d_t^2 \cdot n_{tb}) + \pi \cdot d_t \cdot P_f \cdot n_{tb}](n_{plate} - 1) \tag{A.5}$$

where $W_f = P_t \cdot n_{tb}/n_r$ and $T_f = P_l \cdot n_r$.

The water side area:

$$A_w = \pi d_e \cdot L_{te} \cdot n_{tb} \cdot n_d \tag{A.6}$$

The air side pressure losses coefficients:

$$\sum k_i = k_{ci} + k_{HE,\theta} + k_{to} + k_{sup} \tag{A.7}$$

Inlet contraction loss coefficient, k_{ci}:

$$k_{ci} = 0.05 \tag{A.8}$$

The pressure loss coefficient for a delta heat exchanger, $k_{HE,\theta}$, ([29]):

$$k_{HE,\theta} = k_{HE,t} + (1/sin(\Theta_m) - 1) \cdot [1/sin(\Theta_m) - 1 + 2\sqrt{k_{ci}}] + k_d \tag{A.9}$$

where the loss coefficient across the heat exchanger $k_{HE,t}$, can be calculated as the pressure drop during isothermal flow conditions, k_{HE}, and the term due to the acceleration owing to the density variation due to the non-isothermal operation, $K_{HE,\rho}$:

$$k_{HE,t} = k_{HE} + k_{he,\rho} \tag{A.10}$$

where

$$k_{HE} = K_{HE} \cdot \left(\frac{\dot{m}_a}{\mu_{a,23} A_{fr}} \right)^{b_k} \tag{A.11}$$

and $K_{HE} = 1383.94795\,(m^{-b_k})$ and $b_k = -0.332458$ [29].

To calculate the non-isothermal term, $K_{he,\rho}$:

$$k_{he,\rho} = \frac{2}{\sigma^2}\left(\frac{\rho_{a,2} - \rho_{a,3}}{\rho_{a,2} - \rho_{a,3}}\right) \tag{A.12}$$

Moore's correlation ([29]) was used to calculate the downstream loss coefficient, k_d:

$$k_d = e^{(5.488405 - 0.2131209\Theta + 3.533265\cdot 10^{-3}\Theta^2 - 0.2901016\cdot 10^{-4}\Theta^3)} \tag{A.13}$$

where Θ is the semiangle of the delta columns, and , Θ_m is the mean incidence flow angle:

$$\Theta_m = 0.0019\Theta^2 + 0.9133\Theta - 3.1558 \tag{A.14}$$

The exit loss coefficient, k_{to}:

$$k_{to} = -0.129 \cdot (Fr \cdot D_5/D_3)^{-1} + 0.0144 \cdot (Fr \cdot D_5/D_3)^{-1.5} \tag{A.15}$$

where Fr is the air Froude number:

$$Fr = (\dot{m}_a/A_5)^2/(\rho_{a,5} \cdot (\rho_{a,6} - \rho_{a,5}) \cdot g \cdot D_5); \tag{A.16}$$

and $g = 9.81$ m/s^2.

The tower support pressure loss coefficient:

$$k_{sup} = C_{dts} L_{ts} n_{sup}/(\pi D_3 L_{ts}) \tag{A.17}$$

where C_{dts} is the drag coefficient support (C_{dts} = 2.0), L_{ts} the length of the tower supports and n_{ts} the number of tower supports.

The pressure drop in the cooling circuit:

$$\dot{W}_{p,HE} = (\dot{m}_w/\rho_w)\Delta p_{HE}\, L_t \cdot n_{wp} \cdot K/\eta_{pump} \tag{A.18}$$

$$\dot{W}_{dis} = (\dot{m}_w\, f_{dw} v_w^2/(2d_w)) \cdot (R_{field} + \Delta r_{field}) \cdot 2/\eta_{pump} \tag{A.19}$$

where d_w is the internal diameter of the pipe of the cooling circuit (d_w = 1.5 m).

$$\dot{W}_H = \dot{m}_w g\, L_t/\eta_{pump} \tag{A.20}$$

$$\dot{W}_p = \dot{m}_w/\rho_w(p_1 - p_{a,1})/\eta_{pump} \tag{A.21}$$

where $p_1 = p_{a,1} + \Delta p + p_c + \rho_w 9.81\, L_t + (f_{dw}\rho_w\, v_w^2/(2d_w)) \cdot (R_{field} + \Delta r_{field}) \cdot 2$, and

Volume of the tower shell:

$$V_t = \frac{1}{3}\cdot\pi\cdot H_5\cdot\left[\left(\frac{D_3}{2}\right)^2 + \frac{D_3}{2}\cdot\frac{D_5}{2} + \left(\frac{D_5}{2}\right)^2 - \left(\frac{D_3}{2} - t_s\right)^2 - \left(\frac{D_3}{2} - t_s\right)\cdot\left(\frac{D_5}{2} - t_s\right) - \left(\frac{D_5}{2} - t_s\right)^2\right] \tag{A.22}$$

Table A.7: Cost data used in this study. Sources: [1]Tri City Ready Mix Ltd. [44]. [2] Zou et al. [39] [3]Conradie [30]. [4]Ashwood and Bharathan [46]

Parameter	**Value**
Unit cost of concrete, C_{conc} (\$/m^3)	200[1]
Unit cost of steel, Cu_{steel} (\$/m^3)	1.5[2]
Unit cost of aluminium, Cu_{al} (\$/kg)	5[2]
Added fabrication cost of fins, C_{af} (\$)	0.3[2]
Added fabrication cost of tubes, C_{at} (\$)	3[2]
Pump fixed costs, $C_{pump,fx}$ (\$)	2300[3]
Pump unit costs, $C_{u,pump}$ (\$/W)	180[3]
Direct contact condenser cost, C_{DC} (M\$)	0.42[4]
Heat exchanger factor, f_{he}	1.2[2]
Structural maintenance weighting factor, $f_{st,maint}$	1.2[2]
Foundation factor, f_{found} (\$/m)	22,372 [2]
Ratio of the cost of tower supports to foundation cost, $f_{support}$	0.08[3]
Tower labour costs factor, $f_{tow,labour}$	0.5[3]
Heat exchanger labour costs factor, $f_{HE,labour}$	0.8[3]
Motor factor, f_m	1.1[2]

Appendix B.

The following table shows the energy balance of the power block cycle at the design conditions.

Table B.8: Steam properties for the power block at design conditions (see figure 2).

State	Mass flow rate $\dot{m}$ (kg/s)	Enthalpy h (kJ/kg)	Pressure P (bar)	Temperature T (K)
1	87.46	3475.1	126	823.15
2	87.46	3149	35.98	642.4
3	81.71	3565.5	34.18	823.15
4	3.94	3406.2	20.06	745
5	4.11	3235.7	10.61	660.1
6	3.71	3049	4.95	565.5
7	3.65	2870.3	20.99	473.1
8	3.49	2691.5	0.73	379.1
9	1.71	2514.3	0.20	333.8
10	61.07	2417	0.095	317.9
11	73.65	1834.8	0.09	316.9
12	5.75	939.9	35.98	492.2
13	9.7	811.1	20.06	463.9
14	3.71	528	4.95	398.8
15	7.36	398.4	2.09	368.2
16	10.85	270.5	0.73	337.7
17	12.57	207.3	0.20	322.6
C1	73.65	184.8	11.01	317
C2	73.65	247.9	10.91	332.2
C3	73.65	375.5	10.81	362.6
C4	73.65	504.6	10.71	393.2
C5	73.65	631.7	10.61	422.9
C6	87.46	774	10.61	455.6
C7	87.46	792.2	141.3	458.3
C8	87.46	917.9	140.8	486.6
C9	87.46	1063.2	140	518.3

Hourly performance of the Heller-system and net power produced for three different days.

a)

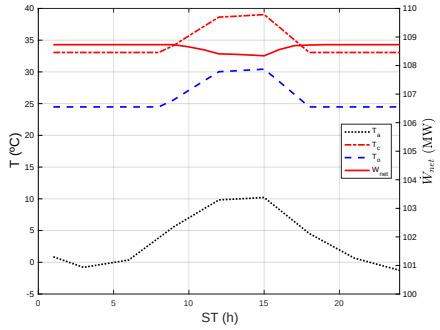

b)

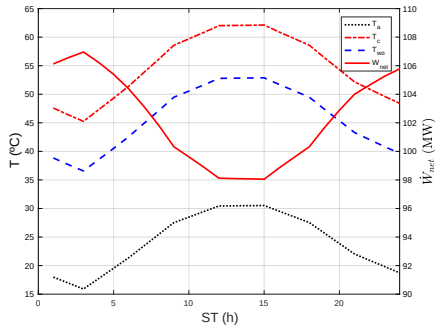

c)

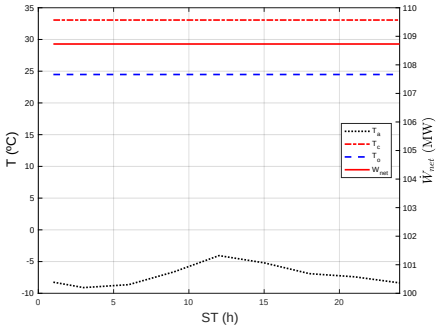

Figure B.10: Power plant performance along a day, for different sunny days: a) 21st of March, b) 21 of June and c) 21 of December. Right axis: temperature (ambient (black dotted), condensing temperature (red-dotted dashed line) and cooling outlet water (blue dashed line) and net power generated in the CSP plant (left axis).

References

[1] R. Goldstein, J. Maulbetsch, Water use for electric power generation, Electric Power Research Institute. EPRI. 1014026, 2008.

[2] NREL, Concentrating Solar Power Projects by Technology, `https://solarpaces.nrel.gov/by-technology/`, accessed: 2019-12-16, 2019.

[3] G. Otieno, A. E. Loosen, An analysis of Key Environmental and Social Risks in the Development of Concentrated Solar Power Projects, in: AIP Conference Proceedings. Proceedings SolarPaces 2015,Cape Town, South Africa, vol. 1734, 160012–1–8, 2016.

[4] N. Bracken, J. Macnick, A. Tovar-Hastings, P. Komor, M. Gerritsen, S. Mehta, Concentrating Solar Power and Water Issues in the U.S. SouthWest, NREL Technical Report. NREL/TP-6A50-61376, 2015.

[5] L. Moreno-Merino, N. Imbern-Fernández, J. J. Durán-Valsero, H. Aguilera, Concentrating solar power plants versus groundwater resources in Mediterranean areas of Spain: The environmental dilemma, Journal of Environmental Management 206 (2018) 409–417.

[6] K. Birkinshaw, M. Masri, R. Therkelsen, Comparison of Alternate Cooling Technologies for California Power Plants. Economic, Environmental and Other Tradeoffs, Electric Power Research Institute. EPRI. 500-02-079F, 2002.

[7] P. Habl, A. M. Blanco-Marigorta, B. Erlach, Exergoeconomic comparison of wet and dry cooling technologies for the Rankine cycle of a

689 solar thermal power plant, in: ECOS2012. The 25^{th} International con-
690 ference on efficiency, cost, optimization and simulation of energy con-
691 version systems and processes, 109–122, 2012.

692 [8] C. Turchi, M. Wagner, C. Kutscher, Water Use in Parabolic Trough
693 Power Plants: Summary Results from WorleyParsons' Analyses,
694 NREL Technical Report. NREL/TP-5500-49468, 2010.

695 [9] M. Martín, Optimal annual operation of the dry cooling system of
696 a concentrated solar energy plant in the south of Spain, Energy 84
697 (2015) 774–782.

698 [10] J. A. Luceño, M. Martín, Two-step optimization procedure for the
699 conceptual design of A-frame systems for solar power plants, Energy
700 165 (2018) 483–500.

701 [11] X. Li, S. Duniam, H. Gurgenci, Z. Guan, V. A., Full scale experimental
702 study of a small natural draft dry cooling tower for concentrating
703 solar thermal power plant, Applied Energy 193 (2017) 15–27 .

704 [12] M. M. Ehsan, X. Wang, Z. Guan, A. Y. Klimenko, Design and perfor-
705 mance study of dry cooling system for 25MW solar power plant op-
706 erated with supercritical CO_2 cycle, International Journal of Thermal
707 Science 132 (2018) 398–410.

708 [13] P. Palenzuela, G. Zaragoza, D. Alarcón-Padilla, J. Blanco, Evaluation
709 of cooling technologies of concentrated solar power plants and their
710 combination with desalination in the mediterranean area, Applied
711 Thermal Engineering 50 (2013) 1514–1521.

712 [14] T. Jászay, The air-cooled condensing equipment ”System Heller”. A
713 comprehensive survey., Industrial review. Aus der Industrie. 2 (4)
714 (no-date) 389–402.

715 [15] J. P. Rossie, E. A. Cecil, Research on dry-type cooling towers for ther-
716 mal electric generation: Part I, Water Quality Office Environmental
717 Protection Agency: Project 16130 EES. Contract 14-12-823., 1970.

718 [16] G. R. Ahmadi, D. Toghraie, Energy and exergy analysis of Montazeri
719 Steam Power Plant in Iran, Renewable and Sustainable Energy Re-
720 views 56 (2016) 454–463.

721 [17] J. Jahangiri, F. Rahmani, Power production limitations due to the
722 environmental effects on the thermal effectiveness of NDDCT in an
723 operating powerplant, Applied Thermal Engineering 141 (2018) 444–
724 455.

725 [18] A. Jahangiri, M. M. Yahyaabadi, A. Sharif, Exergy and economic anal-
726 ysis of using the flue gas injection system of a combined cycle power
727 plant into the Heller Tower to improve the power plant performance,
728 Journal of Cleaner Production 223 (2019) 695–710.

729 [19] A. Colmenar-Santos, D. Borge-Diez, C. Pérez-Molina, M. Castro-Gil,
730 Water consumption in solar parabolic trough plants: review and anal-
731 ysis of the southern Spain case, Renewable and Sustainable Energy
732 Reviews 34 (2014) 565–577.

733 [20] S. Duniam, I. Jahn, K. Hooman, Y. Lu, Veeraragavan, Comparison of
734 direct and indirect natural draft dry cooling tower cooling of the sCO_2

Brayton cycle for concentrated solar power plants, Applied Thermal Engineering 130 (2018) 1070–1080.

[21] I. H. Bell, J. Wronski, S. Quoilin, V. Lemort, Pure and Pseudo-pure Fluid Thermophysical Property Evaluation and the Open-Source Thermophysical Property Library CoolProp, Industrial & Engineering Chemistry Research 53 (6) (2014) 2498–2508, doi: \bibinfo{doi}{10.1021/ie4033999}, URL http://pubs.acs.org/doi/abs/10.1021/ie4033999.

[22] J. Gómez-Hernández, P. A. González-Gómez, J. Briongos, D. Santana, Maximizing the power block efficiency of solar tower plants: Dual-pressure level steam generator, Applied Thermal Engineering 144 (2018) 583–592.

[23] M. J. Montes, A. Abánades, J. M. Martínez-Val, M. Valdés, Solar multiple optimization for a solar-only thermal power plant, using oil as heat transfer fluid in the parabolic trough collectors, Solar Energy 83 (2009) 2165–2176.

[24] R. Srinivasan, Optimum Condenser Cooling Water Temperature Rise in Power Plants, in: ASME (Ed.), Proceedings of IJPGC03, 15–29, 2003.

[25] R. C. Spencer, K. C. Cotton, C. N. Cannon, A method for predicting performance of steam generators:. 16,500 kW and larger, J. Eng. Power 4 (1963) 249–298.

[26] J. Liu, Y. Hu, D. Zeng, W. Wang, Optimization of an air-cooling system and its application to grid stability, Applied Thermal Engineering 61 (2013) 206–212.

[27] R. Chacartegui, D. Sánchez, J. Becerra, A. Muñoz, T. Sánchez, Performance analysis of a 565 MW steam power plant, in: Proceedings of the ASME 2011 Turbo Expo: Turbine Technical Conference and Exposition, vol. 7, 2427–2436, 1982.

[28] W. Harvey, K. Wallace, Geothermal Power Generation. Flash steam geothermal energy conversion systems: Single-, double-, and triple-flash and combined-cycle plants, Elsevier Ltd, 2016.

[29] D. G. Kröger, Air-cooled heat exchangers and cooling towers, Pennwell Corp, Tulsa, Olk, USA, 2004.

[30] A. E. Conradie, Performance optimization of engineering system with particular reference to dry-cooled power plants, PhD Thesis. Stellenbosch (South Africa). University of Stellenbosch, 1995.

[31] M. Takahashi, A. K. Nayak, S.-i. K. Hiroyuki Murakoso, Heat Transfer in Direct Contact Condensation of Steam to Subcooled Water Spray, Journal of Heat Transfer 123 (2001) 703–710.

[32] H. Wei, Z. Ge, L. Yang, X. Du, Entransy based optimal adjustment of louvers for anti-freezing of natural draft dry cooling system, International Journal of Heat and Mass Transfer 134 (2019) 468–481.

[33] X. Yang, H. Wei, R. Jin, L. Yang, X. Du, Y. Yang, Anti-freezing of air-cooled heat exchanger with rolling-type windbreaker, International Journal of Heat and Mass Transfer 136 (2019) 70–86.

[34] W. Wang, Y. Kong, X. Huang, L. Yang, X. Du, Y. Yang, Anti-freezing of air-cooled heat exchanger by switching off sectors, Applied Thermal Engineering 120 (2017) 327–339.

[35] F. Mayinger, A. Chávez, Measurements of direct-contact condensation of pure saturated vapour on an injection spray by applying pulsed laser holography, International Journal of Heat and Mass Transfer 35 (3) (1992) 691–702.

[36] W. Roetzel, F. J. L. Nicole, Mean Temperature Difference for Heat Exchanger Design- A general approximate explicit equation, Journal of Heat Transfer 97 (1975) 5–8 .

[37] A. M. Lu, Small Natural Draft Dry Cooling Towers for Renewable Power Plants, PhD Thesis, 2014.

[38] K. Wilber, J. Maulbetsch, Air-Cooled Condenser Design, Specification, and Operation Guidelines, Electric Power Research Institute. EPRI. 1007688, 2005.

[39] Z. Zou, Z. Guan, H. Gurgenci, Optimization design of solar enhanced natural draft dry cooling tower, Energy Conversion and Management 76 (2013) 945–955.

[40] Y. Yang, L. Chen, X. Du, Y. Yang, Effects of ambient winds on the

thermo-flow performances of indirect dry cooling system in a power plant, International Journal of Thermal Sciences 64 (2013) 178–187.

[41] PVGIS, PHOTOVOLTAIC GEOGRAPHICAL INFORMATION SYSTEM, http://re.jrc.ec.europa.eu/pvg_tools/en/tools.html, accessed: 2019-12-16, 2019.

[42] A. Balohg, Z. Szabó, Heller system: the economical substitute for wet cooling - to avoid casting a shadow upon the sky, in: EPRI Workshop on Advance Thermal Electric Power cooling Technologies. July 8-9, 2008, Charlotte (NC). USA, 2008.

[43] J. Kloppers, D. G. Kröger, Cost optimization of cooling tower geometry, Engineering Optimization 36:5 (2004) 575–584.

[44] Tri City Ready Mix Ltd., Tri City Ready Mix Ltd., {https://tricityreadymix.com/price-list/}, accessed: 2019-09-30, 2019.

[45] CEA, Report on minimisation of water requirement in coal based thermal power stations, http://www.cea.nic.in/reports/others/thermal/tetd/min_of_20water_coal_power.pdf, accessed: 2020-02-25, 2012.

[46] A. Ashwood, D. Bharathan, Hybrid Cooling Systems for Low-Temperature Geothermal Power Production, NREL Technical Report. NREL/TP-5500-48765, 2011.

[47] K. Damerau, K. Williges, A. G. Patt, P. Gauche, Costs of reducing water use of concentrating solar power to sustainable levels: Scenarios for North Africa, Energy Policy 39 (2011) 4391–4398.

[48] U.S. Department of Energy, Concentrating Solar Power Commercial Application Study: Reducing Water Consumption of Concentrating Solar Power Electricity Generation, (DOE), 2008.

[49] U.S. Energy Information administration, U.S. Energy Information administration, {eia.gov}, accessed: 2019-10-08, 2019.

[50] J. Maulbetsch, M. N. DiFilippo, Cost and value of water use at combined-cycle power plants, CEC-500-2006-034, 2006.

[51] NREL, Linear Fresnel Reflector Projects, https://solarpaces.nrel.gov/by-technology/linear-fresnel-reflector, accessed: 2019-07-26, 2019.

[52] Y. Q. Kong, L. J. Yang, X. Z. Du, Y. P. Yang, Air-side flow and heat transfer characteristics of flat and slotted finned tube bundles with various tubes pitches, International Journal of Heat and Mass transfer 99 (2016) 357–371.